Nonlinear dynamics of intermittent-contact mode atomic force microscopy

J. Berg and G. A. D. Briggs
Department of Materials, Oxford University, Parks Road, Oxford OX1 3PH, Great Britain
(Received 8 October 1996)

In intermittent-contact mode atomic force microscopy (AFM), the AFM tip and the harmonically driven sample only spend a brief time in contact, compared to the driving period. As a result the dynamical response of the cantilever to the shocks received on impact can be described and analyzed in terms of an instantaneous impact law specifying the loss of kinetic energy on impact. The simplest such law assumes a constant coefficient of restitution and results in the impact oscillator model. The coefficient-of-restitution law is modified to include an absolute loss of energy on impact, modeling the effects of adhesion. The stability of single-impact orbits for this impact law is analyzed. The analytical results based on these models are found to be in agreement with experiment. A model of the tip-sample interaction based on the Johnson-Kendall-Roberts model of contact incorporating the effects of a liquid meniscus between the tip and the sample is presented. The resulting impact law is found to follow the modified impact law in the presence of adhesion. [S0163-1829(97)06121-8]

I. INTRODUCTION

Since its inception[1] atomic force microscopy (AFM), which employs a nanosized tip on the end of a cantilever to sense the interaction between the tip and a sample, has incurred a wide range of applications.[2] Simultaneously, a plethora of different techniques based on the AFM principle have been developed for a wide range of purposes.[3] In particular several dynamic techniques where the AFM tip, cantilever base, or the sample are subjected to a periodic excitation have been used for a number of applications. Different modes of AFM operation may be set up according to the frequency and amplitude of the vibration applied and the AFM component it is applied to.[4]

In this paper we will use the tools of dynamic systems theory (nonlinear dynamics) to analyze the dynamics of intermittent contact mode AFM. Whereas this mode has been studied recently using mainly numerical techniques,[5–11] the emphasis in this paper lies on simplified partially analytically soluble models. It is found that the amplitude of vibration of the tip in intermittent contact mode is sensitive to the loss of kinetic energy of the tip on impact, and may thus be used to characterize local energy dissipation on the sample.

In intermittent contact mode AFM the sample or cantilever is harmonically driven at an amplitude sufficiently large for the tip to undergo impacts with the sample and to perform a ''bouncing'' motion between impacts. In the following we consider the case where the sample, rather than the cantilever, is harmonically driven, since this case is mathematically and conceptually simpler. The case where the cantilever is driven is obtained by the noninertial transformation to the frame where the sample is at rest. The impacts are assumed to be brief, so that the tip is out of contact with the sample for most of its motion. If the duration of impact is short compared to the driving period of the sample, the relative velocity of tip and sample after impact is a function of their relative velocity before impact. Otherwise no such impact law representing the energy loss on impact may hold due to the acceleration of the sample during impact. The brevity of impact results from the highly nonlinear increase in stiffness on impact—from the stiffness of the cantilever to that of the tip-sample contact. Thus instead of treating the response of the tip-cantilever system in the presence of the sample as a perturbation to the linear, and hence harmonic, behavior, models are considered which are inherently nonlinear. As a result the language and tools of dynamic systems theory become applicable. The experimental justification for such an approach stems from recent work,[12] where the AFM was excited at frequencies several times higher than that of the the free cantilever. Both subharmonic orbits of a period several times that of the excitation as well as chaotic motion of the tip were observed.

Throughout, the single-mass model will be used to describe the tip-cantilever system. It has been used extensively to model both contact, noncontact, and intermittent contact AFM.[4] In the noncontact and intermittent-contact case there is good agreement with experiment. The single-mass model assigns the tip and cantilever a single effective mass and stiffness, thus neglecting any higher modes of vibration of the cantilever. Figure 1 shows a schematic representation of the cantilever and the tip and their description by the single-mass model.

II. THE IMPACT OSCILLATOR

The so-called impact oscillator is a prototype model of vibrating systems undergoing rigid impacts, which has been extensively studied.[13–15] It has been used to model processes where harmonically forced systems undergo impacts with a rigid constraint in fields as diverse as the effects of earthquakes on rigid structures[16] or offshore engineering.[17,18] As a result the impact oscillator still remains the subject of considerable theoretical, computational, and experimental interest today.[19]

It consists of a harmonically driven harmonic oscillator undergoing impacts with an infinitely rigid object. These impacts are assumed to occur instantaneously and obey the coefficient-of-restitution rule of impact: On impact the veloc-

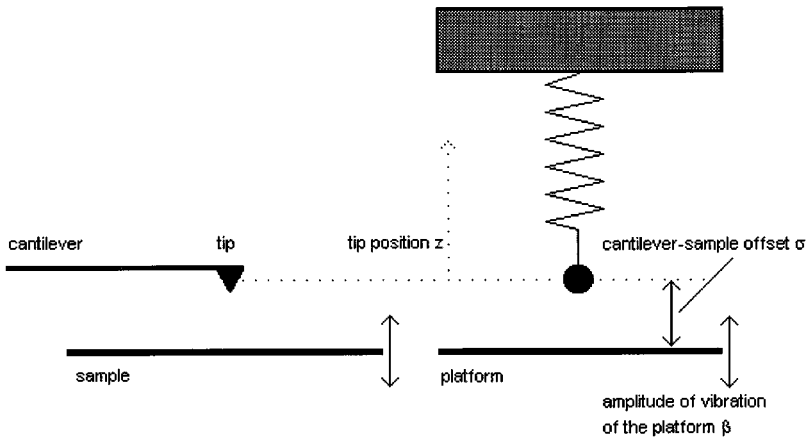

FIG. 1. Schematic representation of the AFM setup with sample modulation and the corresponding single-mass model with the tip at its equilibrium position.

ity of the oscillator is reversed and multiplied by a constant factor r, the coefficient of restitution. In general $r \leqslant 1$, where the equality applies to the case of perfectly elastic impacts. Hence the oscillator loses a constant fraction $1-r^2$ of its kinetic energy on impact.

The motion of the oscillator can be described by two regimes; a linear equation of motion between impacts, and the discontinuous instantaneous impact law. The impact oscillator exhibits a behavior of fascinating complexity,[20] and, depending on the driving frequency and amplitude, its motion may be periodic or chaotic. The periodic motion is classified according to the number of impacts per period m, and the number of driving cycles per period n. Such a type of motion is denoted as an (m,n) orbit, where m and n are integers. Chaotic motion may occur due to the nonlinearity introduced by the impact law: The motion of the oscillator between impacts is given by the linear equation of motion and the initial conditions set at the *previous* impact. In this way it is possible for the initial conditions when starting off the oscillator never to be damped out, although energy is being dissipated. Such a sensitivity on initial conditions is one of the hallmarks of chaotic dynamics.

By transforming the equations governing the behavior of the impact oscillator to the frame of reference where the oscillator is unforced but the *obstacle* is performing simple harmonic motion, we arrive at the single-mass model as shown in Fig. 1 subject to a coefficient-of restitution rule of impact.

In order to describe the dynamics of this system, we define its Poincaré section as the surface $\{z,\dot{z},t: z=z_p,\dot{z}>0\}$, where z is the position of the tip relative to the lab frame, $\dot{z}$ is its velocity and $z_p=\sigma+\beta\cos(\omega t)$ is the position of the platform. Hence the Poincaré map maps the velocity immediately after impact and the time of impact from one impact to the next. Throughout we will refer to the velocity of the tip just after impact as the impact velocity, which is thus positive. The phase flow is transverse to the Poincaré section everywhere except where $\dot{z}=0$. Since the driving term is periodic with period $2\pi/\omega$, we may reduce the phase space to the topology of a cylinder. The corresponding mapping maps the impact velocity and time modulo the driving period from one impact to the next.

In the lab frame, where the platform velocity is $\dot{z}_p=-\beta\omega\sin(\omega t)$, the coefficient of restitution law of impact gives

$$\dot{z}\rightarrow -r\dot{z}-(1+r)\beta\omega\sin(\omega t). \tag{1}$$

When determining the stability of single-impact orbits, use is made of the fact that the equation of motion *between* consecutive impacts is linear and its solution as well as its derivatives with respect to the time of impact and impact velocity can be given in closed form.

Consider two consecutive impacts at times t_1 and t_2. Denoting signed velocities just before impact as V and just after impact as V' and neglecting damping, the motion of the mass between these impacts is given by

$$z(t)=A\cos\Omega(t-t_1)+B\sin\Omega(t-t_1), \tag{2}$$

where the initial conditions give

$$A=\sigma+\beta\cos(\omega t_1),$$

$$B=V_1'/\Omega.$$

The impact time t_2 is given implicitly by the condition

$$A\cos\Omega(t_2-t_1)+B\sin\Omega(t_2-t_1)=\sigma+\beta\cos(\omega t_2), \tag{3}$$

which is called a *switching condition*, because the coefficients in the analytic solution (2) for subsequent times switch to new values given by new initial conditions. The velocity just before impact is given by

$$V_2=-A\Omega\sin\Omega(t_2-t_1)+B\Omega\cos\Omega(t_2-t_1). \tag{4}$$

Phrased in terms of the Poincaré section the stability of single-impact orbits can be determined by linearizing the Poincaré map about its fixed points. For a general two-dimensional map with the variables t_k and V_k' and a fixed point t^*, V'^* we can write

$$\delta t_{k+1}\approx \frac{\partial t_{k+1}}{\partial t_k}\delta t_k+\frac{\partial t_{k+1}}{\partial V_k'}\delta V_k',$$

$$\delta V_{k+1}'\approx \frac{\partial V_{k+1}'}{\partial t_k}\delta t_k+\frac{\partial V_{k+1}'}{\partial V_k'}\delta V_k',$$

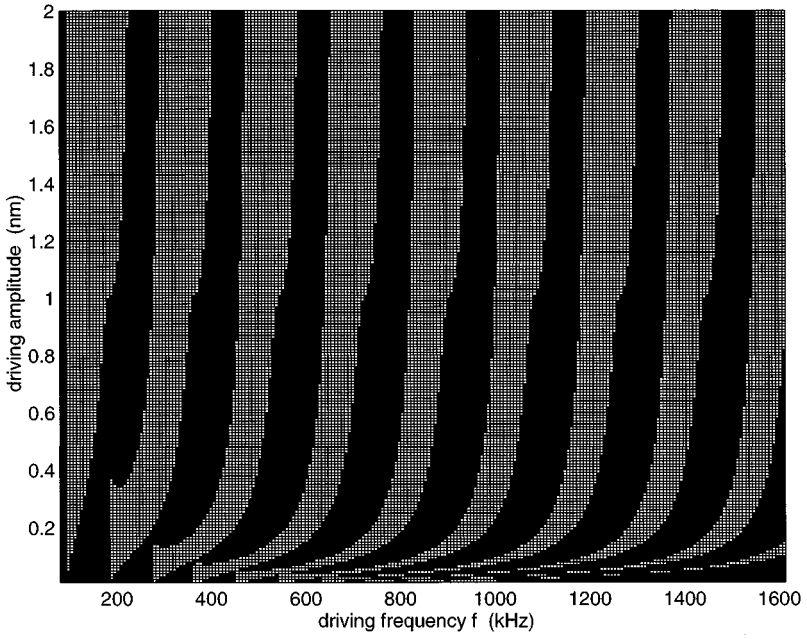

FIG. 2. Regions of stability of single-impact orbits are shown white. $\Omega=90\times 2\pi$ kHz, $r=0.5$, and $\sigma=-1$ nm.

to first order in the small deviations δt and $\delta V'$ from the fixed point. The partial derivatives form the Jacobian matrix $\partial(t_{k+1},V'_{k+1})/\partial(t_k,V'_k)$ of the mapping, which describes the linearized behavior of points near the fixed point under the Poincaré map. If the absolute values of the eigenvalues of this matrix are all smaller than 1, there exists an attractive neighborhood around the fixed point within which application of the Poincaré map brings all points closer to the fixed point. Hence the corresponding orbit is stable.[21] Since the criterion that the modulus of the eigenvalues be smaller than 1 can be written as $|T|<|D+1|$, the stability of single-impact orbits can be determined by finding the determinant D and trace T of the Jacobian matrix of the Poincaré map. Implicitly differentiating Eqs. (3) and (4) gives $\partial(t_{k+1},V_{k+1})/\partial(t_k,V'_k)$ and applying the chain rule and the coefficient of restitution law (1) gives the elements of the Jacobian matrix.

The results of the first part of this calculation are

$$\left(\frac{\partial t_2}{\partial t_1}\right)_{V'_1}=\frac{-\beta\omega s_1\mathcal{C}+A\Omega\mathcal{S}-B\Omega\mathcal{C}}{A\Omega\mathcal{S}-B\Omega\mathcal{C}-\beta\omega s_2},$$

$$\left(\frac{\partial t_2}{\partial V'_1}\right)_{t_1}=\frac{\mathcal{S}/\Omega}{A\Omega\mathcal{S}-B\Omega\mathcal{C}-\beta\omega s_2},$$

$$\left(\frac{\partial V_2}{\partial t_1}\right)_{V'_1}=\beta\omega\Omega s_1\mathcal{S}-\Omega^2(A\mathcal{C}+B\mathcal{S})\times\frac{\beta\omega(s_2-s_1\mathcal{C})}{A\Omega\mathcal{S}-B\Omega\mathcal{C}-\beta\omega s_2},$$

$$\left(\frac{\partial V_2}{\partial V'_1}\right)_{t_1}=\mathcal{C}-\frac{\Omega(A\mathcal{C}+B\mathcal{S})\mathcal{S}}{A\Omega\mathcal{S}-B\Omega\mathcal{C}-\beta\omega s_2}, \tag{5}$$

where $\mathcal{C}=\cos\Omega(t_2-t_1)$, $\mathcal{S}=\sin\Omega(t_2-t_1)$ and $c_{1/2}=\cos(\omega t_{1/2})$, $s_{1/2}=\sin(\omega t_{1/2})$.

By computing the Jacobian of Eq. (1) and applying the chain rule the determinant D and the trace T of the Jacobian of the Poincaré map can be calculated and the stability of single-impact orbits be determined.[13] Regions of stability in the (ω,β) plane are shown in Fig. 2. They are found to consist of resonances centered on $\omega=2n\Omega$, that is, orbits where half a period of the free motion of the tip equals n driving periods. At low driving frequencies ''tails'' of regions of stability slope towards lower/higher driving frequencies for a negative/positive sample-cantilever offset σ.

III. THE COEFFICIENT-OF-RESTITUTION RULE INCORPORATING ADHESION

We now extend the coefficient of restitution rule (1) to include not only a constant *fractional* loss of energy on impact but also a constant *absolute* loss δ of kinetic energy after application of Eq. (1). This can be thought of as a crude model of the effects of adhesion. In the frame of reference where the platform position is $z_p=\sigma+\beta\cos(\omega t)$ this modified impact rule gives

$$V'=\sqrt{r^2(V-v_p)^2-\epsilon}+v_p, \tag{6}$$

where V and V' are the tip velocities just before and just after impact respectively, and v_p is the velocity of the platform on impact. ϵ is a shorthand for $2\delta/m$, where m is the effective mass of the tip. We determine the stability of single impact orbits by calculating the determinant D and trace T of the Jacobian matrix $\partial(t_2,V'_2)/\partial(t_1,V'_1)$ of the Poincaré map. The elements of $\partial(t_2,V_2)/\partial(t_1,V'_1)$ are given by Eq. (5), whereas the elements of the Jacobian $\partial(t_2,V'_2)/\partial(t_2,V_2)$ of the modified impact law (6) are

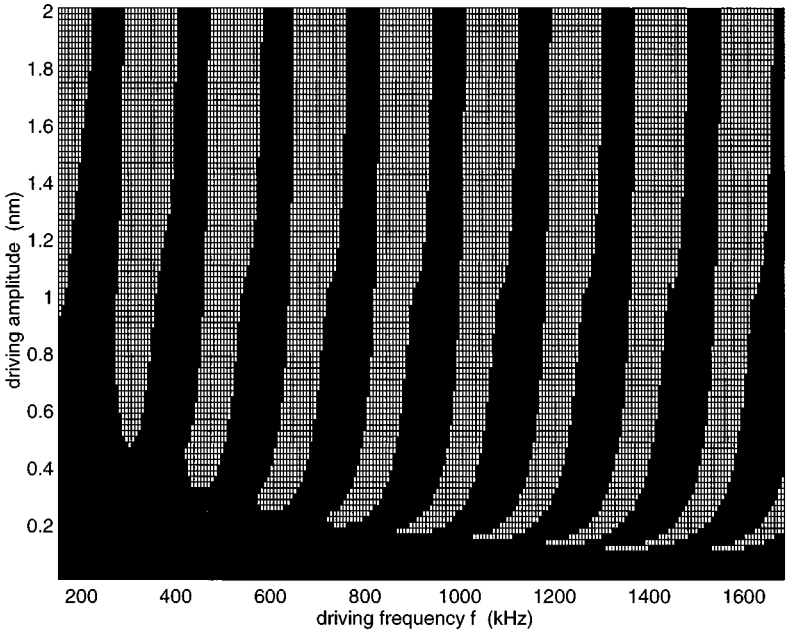

FIG. 3. Regions of stability of single-impact orbits in the presence of adhesion.

$$\left(\frac{\partial t_2}{\partial t_2}\right)_{V_2}=1,$$

$$\left(\frac{\partial V_2'}{\partial t_2}\right)_{V_2}=\beta\omega^2\cos(\omega t_2)\left(\frac{r^2(V_2-v_{p(2)})}{\sqrt{r^2(V_2-v_{p(2)})^2-\epsilon}}-1\right),$$

$$\left(\frac{\partial t_2}{\partial V_2}\right)_{t_2}=0,$$

$$\left(\frac{\partial V_2'}{\partial V_2}\right)_{t_2}=\frac{r^2(V_2-v_{p(2)})}{\sqrt{r^2(V_2-v_{p(2)})^2-\epsilon}}, \tag{7}$$

where $v_{p(2)}=-\beta\omega\sin(\omega t_2)$ denotes the platform velocity at the second impact. Using Eqs. (5) and (7) the chain rule is applied again to calculate the Jacobian matrix of the Poincaré map

$$\frac{\partial(t_2,V_2')}{\partial(t_1,V_1')}=\frac{\partial(t_2,V_2')}{\partial(t_2,V_2)}\,\frac{\partial(t_2,V_2)}{\partial(t_1,V_1')}.$$

For a single impact orbit obeying $V_1'=V_2'$ and $v_{p(1)}=v_{p(2)}$ we find for its determinant D and its trace T

$$D=r^2$$

$$\begin{aligned}T&=1+\frac{1}{v_p-V}\left[\beta\omega s-\beta\omega s\mathcal{C}-(V'+\beta\omega s\mathcal{C})r^2\right.\\&\left.\times\frac{V-v_p}{V'-v_p}+\beta\frac{\omega^2}{\Omega}c\mathcal{S}\left(r^2\frac{V-v_p}{V'-v_p}-1\right)\right]\\&=1+\frac{1}{1+\alpha}\left[\mathcal{C}-1+r^2(\alpha-\mathcal{C})\frac{\alpha+1}{\alpha-1}\right.\\&\left.+\frac{\omega}{\Omega}\cot(\omega t)\mathcal{S}\left(r^2\frac{\alpha+1}{\alpha-1}+1\right)\right],\end{aligned} \tag{8}$$

where indices have been dropped, $\alpha=V'/v_p$, and the rest of the notation follows that of Sec. II.

In order to evaluate Eq. (8) the impact phase (ωt) must be calculated. Equating the n periods of the platform with that of the tip motion in a $(1,n)$ orbit, we obtain $V'=[\sigma+\beta\cos(\omega t)]\Omega\tan(\pi n\Omega/\omega)$, and solving Eq. (6) for V' for the case of a single-impact orbit gives

$$\frac{(1+r^2)v_p+\sqrt{4r^2v_p^2-(1-r^2)\epsilon}}{1-r^2}$$

$$=[\sigma+\beta\cos(\omega t)]\Omega\tan(\pi n\Omega/\omega). \tag{9}$$

The presence of the square root on the left-hand side of this equation, which stems from the square root in the modified impact law (6), leads to a polynomial equation of fourth order in $\cos(\omega t)$, which must be solved numerically. Hence expressions (8) can be evaluated and the stability criterion $|T|<|1+D|$ can be applied.

Figure 3 shows the results of this calculation for $\sigma=-1$ nm, $r=0.5$, $\epsilon=1\ \mu\mathrm{J\,kg^{-1}}$. The regions of stability of single impact orbits are similar to those of the simple coefficient of restitution law, except at low driving amplitudes and subharmonic orbits of low order. This stems from the fact that the impact rule (6) does not allow orbits with $V-v_p<\sqrt{\epsilon}/r$, i.e., $v_p<\sqrt{\epsilon}/r(\alpha+1)$, since $v_p\sim\beta n$ subharmonic orbits of low order and low driving amplitude cannot occur under the modified impact rule. This corresponds to the tip getting stuck by adhesion.

Note that the fundamental frequency in the power spectrum of a $(1,n)$ orbit is $1/n$ of the driving frequency and the orbit is hence termed subharmonic of order n. The order in which the subharmonics appear as the driving amplitude is increased is related to the tip-sample offset parameter σ and for negative σ Figs. 2 and 3 show that high order subharmonic orbits occur before the lower orders with re-

gions where no single impact orbits are stable between them. This behavior agrees with the experimental results reported in Ref. 12.

IV. NUMERICAL SIMULATIONS INCORPORATING THE EFFECT OF A LIQUID MENISCUS

In this section we construct a model of the tip-sample interaction, focusing on the dissipation of energy on impact. Since impacts are brief compared to the driving period it is the energy dissipation rather than the contact mechanics which is paramount to the dynamics of the tip. As long as the elastic forces acting on the tip on contact result in a sufficiently large acceleration for impacts to be brief, the relation between the tip velocities before and after impact is crucial, but not the exact form of quasistatic forces reversing the tip velocity. This is reflected in the model of the tip-sample interaction, which includes the effects of a liquid meniscus between tip and the sample. Such a meniscus is ubiquitous in AFM under ambient conditions and its viscosity contributes to the energy dissipation on impact.

The model is composed of two parts, the liquid/solid contact describing the force exerted by a liquid meniscus between the tip and the sample, and the solid/solid contact describing the case when the tip is in direct elastic contact with the sample. Both regimes are well researched on their own (Refs. 22,23, and references contained therein), but the interface between these continuum theories is likely to be dominated by the molecular dynamics of the tip-meniscus-sample system and is currently not well understood. The following thus represents a compromise aimed to describe the dissipation of energy on impact, not the complete contact mechanics of the tip-sample system in the presence of a mesoscopic amount of water. In this sense the prime objective of the quasistatic contribution to the tip-sample interaction—apart from providing the crucial nonlinearity of contact—is to enable the energy dissipation due to velocity-dependent terms to be calculated. As a result, long-range van der Waals forces in air, which do not contribute to the energy loss, are neglected. The forces describing the liquid bridge are the capillary force, the viscous force, the structural force, and the core repulsion. The solid/solid contact is described by the Johnson-Kendall-Roberts (JKR) model,[24] providing a high tip-sample stiffness due to elastic deformation, as well an energy loss due to adhesive forces.

The capillary force results from the surface tension and hydrostatic forces in a discrete liquid bridge between particles. By considering the total surface energy for a sphere of radius R and a flat connected by a liquid meniscus of constant volume the capillary force is found to be[22,25]

$$F_{\mathrm{cap}}=-\frac{4\pi R\gamma_l}{1+D/2r_K}, \tag{10}$$

where we have assumed the angle at which the meniscus touches the sphere to be close to zero. R is taken equal to 100 nm throughout, γ_l denotes the surface tension of the liquid, D is the tip-sample separation, and r_{K} the Kelvin radius given by[26]

$$r_{\mathrm{K}}=\frac{\gamma_l V_m}{RT\ln(p/p_s)}, \tag{11}$$

where V_m is the molar volume of the liquid, T the temperature, p the pressure, and p_s the saturated vapor pressure. For a water meniscus p/p_s equals the relative humidity. At STP conditions $\gamma_l V_m/RT$ is 0.54 nm for water. In the following calculations the relative humidity is taken to be 50%.

The viscous force arises from the shear viscosity of the liquid as the meniscus is continuously deformed. It has been calculated for a number of geometries and for a sphere of radius R and a flat the result is[25,27]

$$F_{\mathrm{visc}}=-\frac{3\pi\eta_l R^2\dot{D}}{2D}, \tag{12}$$

where $\dot{D}$ is the relative velocity of tip and sample and η_l is the shear viscosity of the liquid. For water at STP conditions $\eta_l=1.005\times10^{-3}$ Pa s.

The structural or entropic force arises from the discrete molecular nature of the liquid meniscus. It is primarily determined by the geometry of the molecules and how they pack around a constraining boundary.[22] When the tip-sample separation is of the order of magnitude of the size of the molecules of the liquid, changes in this separation lead to oscillations of the density of the liquid, and hence to an oscillating force. In this application we consider the average of the structural force over these oscillations. By integrating the expression for the average structural pressure given in Ref. 28 over the area of the meniscus we obtain

$$F_{\mathrm{struct}}=A_0\tau e^{-(D-\delta)/\tau}[1-e^{-a^2/(2R\tau)}], \tag{13}$$

where a is an effective Kelvin radius given by[29]

$$a=R\sin[\cos^{-1}(1-2r_{\mathrm{K}}/R)].$$

The offset δ and the decay length τ of the structural force are both taken to be 0.6 nm, and A_0 equals approximately 40 Nm^{-1}.[28,29]

The core repulsion describes the short-range repulsive force arising from the interaction of the atomic cores of the tip and the sample. They are described by the repulsive part of a Lennard-Jones potential giving

$$F_{\mathrm{core}}=\frac{BR}{180D^8}, \tag{14}$$

where comparison with the van der Waals attraction at $D=0.2$ nm leads to $B=10^{-79}$ J m^{-2}.[29] Figure 4 shows the capillary force, the structural force, and the core repulsion, as well as the sum of these contributions with the parameters given above as a function of tip-sample separation.

In order to describe the forces acting on the tip when in elastic contact with the sample, we use the familiar JKR model of contact,[24] which is well established for the case of high adhesion, large radii of curvature, and compliant materials. The JKR model is based on a balance between surface, potential, and elastic energies, where a constant surface energy $\overline{\omega}$ over the area of contact is assumed. Interaction forces outside the area of contact are not taken into account, leading to infinite stresses along the perimeter of the connective neck between tip and sample.

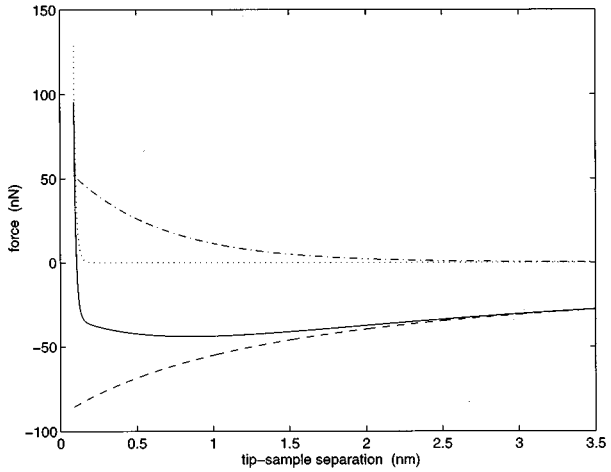

FIG. 4. The constituent forces of the liquid bridge: Capillary force (dashed), structural force (dash-dotted), core repulsion (dotted), and the sum of these contributions (full).

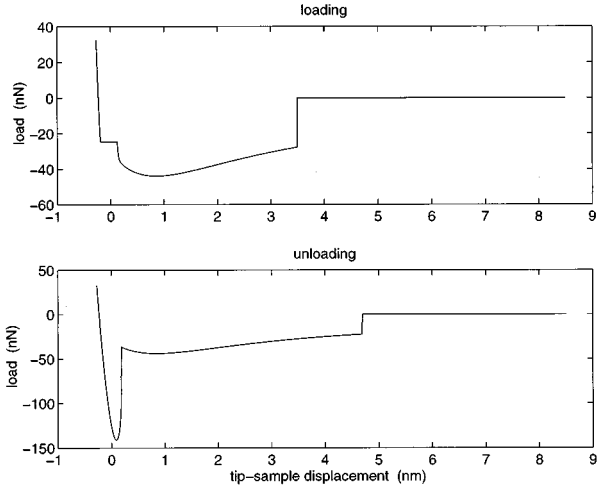

FIG. 5. The loading and unloading curve of the contact model.

Following the notation of Maugis,[30] we use the normalized contact radius A, load P, penetration depth Δ given in terms of the un-normalized variables by

$$A=\frac{a}{[(\pi\overline{\omega}R^2)/K]^{1/3}},$$

$$\overline{P}=\frac{P}{\pi\overline{\omega}R},$$

$$\Delta=\frac{\delta}{[(\pi^2\overline{\omega^2}R)/K^2]^{1/3}},$$

where a is the contact radius, $\overline{\omega}$ the Dupré adhesion energy, P the load, and δ the penetration depth. The reduced elastic modulus K for the tip-sample system is given by

$$\frac{1}{K}=\frac{3}{4}\left[\left(\frac{1-\nu_{\text{tip}}^2}{E_{\text{tip}}}\right)+\left(\frac{1-\nu_{\text{sample}}^2}{E_{\text{sample}}}\right)\right].$$

Using the normalized variables the JKR theory takes the form

$$\overline{P}=A^3-A\sqrt{6A},$$

$$\Delta=A^2-\frac{2\sqrt{6A}}{3} \tag{15}$$

and has to be solved numerically for the relationship between P and Δ. In this application we take $K=100$ GPa and $\overline{\omega}=0.3$ J m^{-2}.

The total force exerted by the liquid bridge is given by the sum of Eqs. (10), (12), (13), and (14). The static components of this force are shown in Fig. 4. For typical impact velocities the viscous force is several orders of magnitude smaller than the static component of the meniscus force. During loading we assume the meniscus to be present for tip-sample displacements smaller than 3.5 nm. Due to the capillary contribution the static force is attractive over most of its range. At distances smaller than about 0.2 nm the structural force and the core repulsion cause the liquid bridge to be repulsive and of large stiffness.[29]

The formation of a solid junction is deemed to occur when the forces and stiffnesses of the solid/solid junction and of the liquid bridge are equal. As shown in Fig. 5 this instability occurs at a tip- sample separation of 0.124 nm and leads to a snap-on at a negative force. The remainder of the loading process is given by the load-displacement relation of the JKR model (15).

However, the microscopic details of the transition from a liquid/solid to a solid/solid contact process are poorly understood as well as difficult to access experimentally. As argued above the exact form of the force curve is not of paramount concern here as long as the correct dissipative processes can be incorporated. However, for applications of contact AFM such as ultrasonic force microscopy an understanding of the transition region may be crucial.[31]

During the unloading process we follow the JKR force curve until the well-known JKR instability occurs and the connective neck between tip and sample breaks. From this point onwards the force is given by the expression for the liquid meniscus, which now extends to greater distances than during the loading process. This distance is taken equal to 4.7 nm yielding a total hysteretic energy loss of 6×10^{-17} J corresponding to a total hysteretic energy loss per unit area of 0.6 J m^{-2}. Both the meniscus and the elastic contact contribute to the total hysteretic energy loss.

The question arises, whether there are further mechanisms of energy loss playing a role, particularly if plastic deformation will occur on impact. However, it is thought that since a repeated number of impacts take place on the same point of the sample, shakedown and strain-hardening[23] will prevent an energy loss due to effects of plasticity after a few impacts.[32] Nevertheless in a situation where the tip is scanned across the surface, permanent damage to the sample may occur and has indeed been observed at driving amplitudes of the order of 10 nm.[33]

A. The impact law

Using the model for the tip-sample interaction developed above to simulate impacts numerically, we can determine the

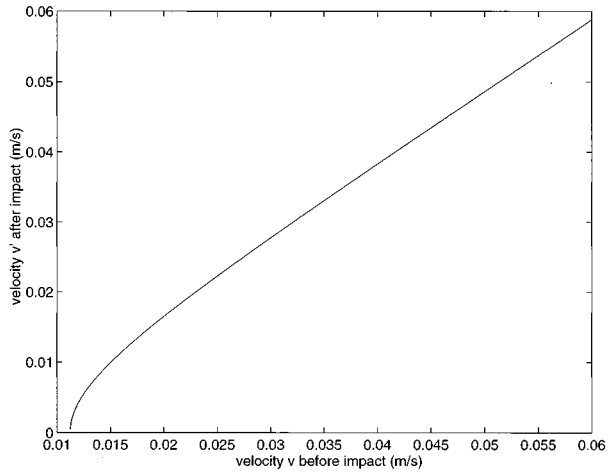

FIG. 6. The impact law resulting from the model of the tip-sample interaction.

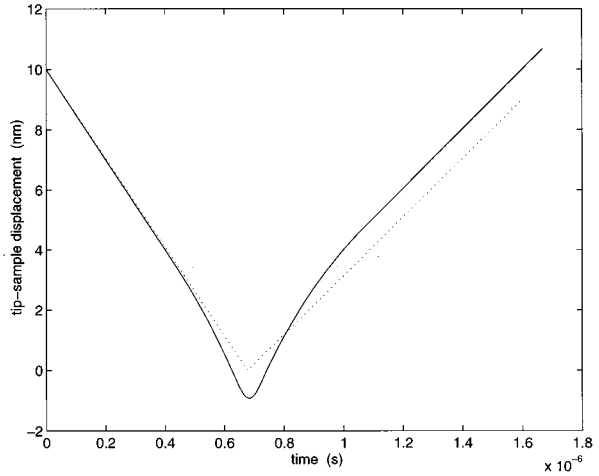

FIG. 7. Distance from the sample against time for a low-velocity impact. Dotted lines show the corresponding trajectory assuming an instantaneous impact.

impact law resulting from this model and examine the assumptions used in Secs. II and III. Throughout a 4/5-order Runge-Kutta algorithm with variable step size is used. In order to find the impact law we consider impacts of a free tip of mass $m=10^{-12}$ kg (Refs. 11,35) on the stationary sample subject only to the forces discussed in Sec. IV. The speeds of the tip at a point further away from the sample than the range of the tip-sample interaction after and before impact, denoted by v' and v respectively, are plotted against each other in Fig. 6. The impact law exhibits a cutoff velocity of 1.12×10^{-2} m s^{-1} corresponding to the tip getting stuck to the sample by adhesion. Figure 6 may be fitted to an impact law of the form $V'=\sqrt{r^2V^2-\epsilon}$, which has been treated in Sec. III. The fit parameters are found to be r = 0.9981 and $\epsilon=1.26\times10^{-4}$m^2 s^{-2} corresponding to an adhesive energy of 6.34×10^{-17} J. This fit reproduces the numerically determined impact law to within 0.3%.

In this context the absolute loss of energy per impact, denoted by ϵ, results from the hysteresis of the force curve. The energy loss related to the kinetic energy of the tip on impact, denoted by the coefficient of restitution r, results from the viscous damping due to the presence of the liquid meniscus between tip and sample. For impact velocities large compared to the cutoff the original coefficient of restitution law $V'=rV$ holds in good approximation.

The assumption behind the application of *any* impact law is that the impact time is so short compared to the driving period that it can be neglected. We can use the model of the tip-sample interaction to examine this assumption. Figure 7 shows the distance of the tip from the sample against time for an impact of velocity $v=1.5\times10^{-2}$ m s^{-1}. Since this impact velocity corresponds to only 1.3 times the velocity cutoff, this is to be considered a low velocity impact. The dotted line shows the corresponding orbit for an instantaneous law of impact. The finite stiffness of the sample introduces a time lag of the numerical solution. For the given impact velocity this lag is 0.11 μs, which is to be compared to the driving period $T=5.5$ $\mu s/n$ to be used below, where n is the order of the subharmonic orbit.[34] Since the stiffness of the JKR model increases with penetration depth, this time lag decreases with increasing impact velocity. Assuming a Hertzian stiffness, to which the JKR stiffness tends for large penetration depths, we immediately find the time lag to scale as $V^{-(1/4)}$.

However, the fact that the hysteretic forces act over a finite range also introduces a time *lead* of the numerical solution with respect to the trajectory given by an instantaneous impact law, since the net loss of energy due to hysteresis takes place during unloading, that is *after* the fictitious ''moment'' of impact assumed by an impact law. For the given impact velocity this time lead is 0.2 μs and from elementary geometrical considerations we find it to scale as V^{-1}. Hence we can conclude in both cases that in the present context the use of an instantaneous impact law is justified for sufficiently large impact velocities. With the parameters of the tip-sample interaction given above, the time spent in contact during an impact of a typical velocity rises to 5% of the driving period for $n=8$, which thus may be regarded as a limit to the validity of the instantaneous-impact approximation. However, this limit is strongly dependent on the values of sample stiffness and effective tip mass chosen.

Using the model of the tip-sample interaction, we can numerically solve the equation of motion of a tip of effective mass m at the end of a cantilever of stiffness k and damping constant γ

$$m\ddot{z}+\gamma\dot{z}+kz=F[(z-z_p),(\dot{z}-\dot{z}_p)], \tag{16}$$

where z and $z_p=\sigma+\beta\cos(\omega t)$ denote the position of the tip and the vibrating platform, respectively. $F[D,\dot{D}]$ gives the tip-sample interaction as a function of their separation D and its rate of change $\dot{D}$. Throughout we take $m=10^{-12}$ kg and consider a cantilever with a free frequency of vibration $\Omega=90$ kHz and a quality factor Q=40.[12,11,35]

Figure 8 shows 1000 points of the Poincaré map defined in Sec. II at parameter values resulting in a chaotic orbit obtained by numerically integrating the equation of motion 16 using a 4/5-order Runge-Kutta algorithm.

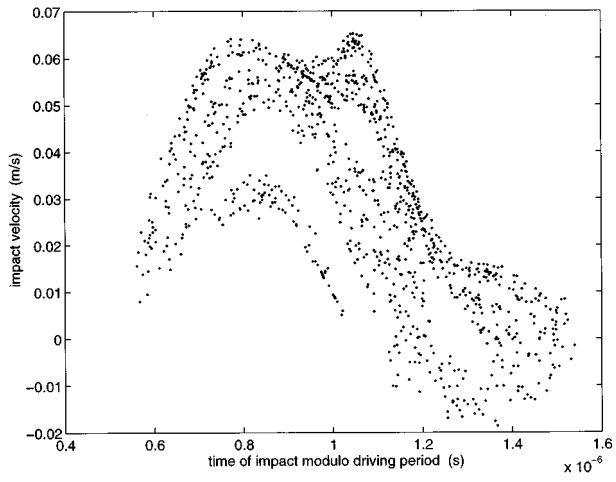

FIG. 8. The strange attractor found by numerically integrating the equation of motion (16) for $n=5.277$, $\beta=4$ nm, and $\sigma=0$.

B. Behavior of the vibration amplitude as the tip-sample offset is decreased

An important procedure, which has been extensively researched experimentally[10] and theoretically[6,11] in the context of intermittent-contact mode AFM, is the slow approach of the periodically driven cantilever base towards the sample. In the setup discussed here this corresponds to gradually increasing the offset σ between the rest positions of the tip and the vibrating sample.[36] At driving frequencies at or near the free resonant frequency of the cantilever an almost linear decrease of the vibration amplitude of the tip is observed, ending with the tip stuck to the sample due to adhesion. This linear decrease in amplitude is found to be fairly independent of the sample properties.

However, we can expect a more interesting behavior to occur at or near single impact resonances of the tip-cantilever system, the first of which occurs at *twice* the free resonant frequency Ω of the cantilever. Furthermore we can compare the predictions of the instantaneous-impact model in this situation with the results of dynamic simulations of the tip-sample interaction.

Using Eq. (9) to find the impact phase, we can determine the amplitude of vibration of stable single-impact orbits—if they exist—just above and below the first resonance, which for $\sigma=0$ occurs at a driving frequency of 2Ω. Figure 9 shows this steady-state amplitude as a function of the tip-sample offset σ and the coefficient of restitution r with $\epsilon=1\,\mu\mathrm{J\,kg^{-1}}$ and the amplitude rescaled to one unit of length at $\sigma=0$. It shows that for a subresonant excitation the amplitude of vibration of the tip decreases linearly only at sufficiently high values of the coefficient of restitution and sufficiently far away from resonance. For an excitation slightly above resonance, the amplitude of vibration is found to *increase* with the cantilever offset. A similar calculation with the driving frequency equal to the free frequency of vibration of the cantilever shows the amplitude of vibration to decrease linearly with σ irrespectively of the coefficient of restitution. Hence the *qualitative* dependence of the amplitude of vibration as σ is varied on the coefficient of restitution is only present near resonance.

This behavior can be understood by considering the impact phase, which decreases as the magnitude of the cantilever-sample offset is decreased. In the subresonant case, where the impact phase lies below $(3/2)\pi$, this implies a lower velocity of the sample at impact and hence a lower steady state amplitude of vibration, and vice versa for the superresonant case. Alternatively we can think of this procedure as shifting the ''tails'' of the regions of stable single-impact orbits in Fig. 3 from lower to higher frequencies, which results in the above effects for orbits just below or above the resonance $\omega=2\Omega$.

If the change in the cantilever-sample offset σ proceeds slowly enough for the system to settle into its new steady state as σ changes, we should expect to observe the same

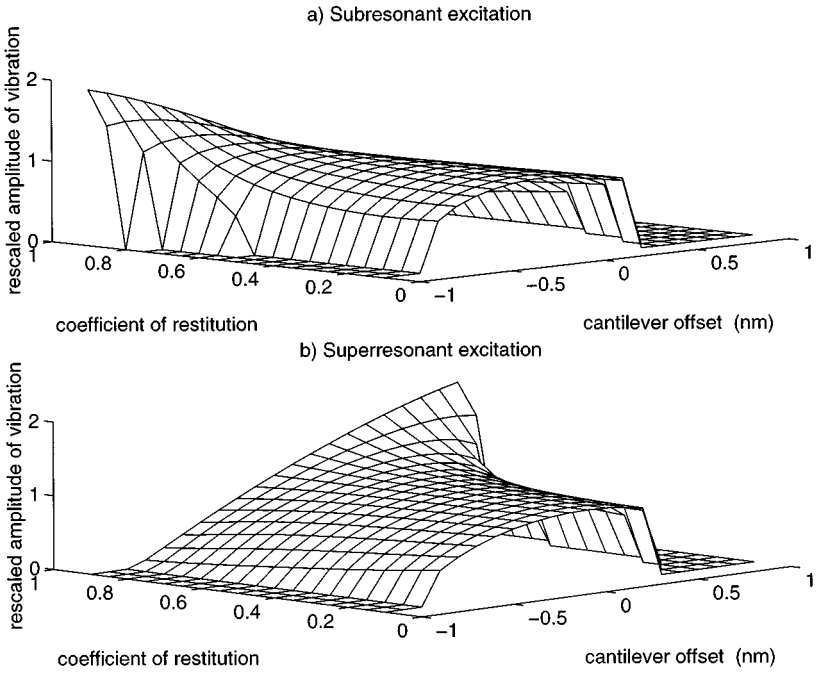

FIG. 9. Amplitude of the single-impact analytic solution of the coefficient of restitution model (a) just below resonance $n=0.97$ and (b) just above resonance $n=1.03$ with a driving amplitude of $\beta=0.75$ nm.

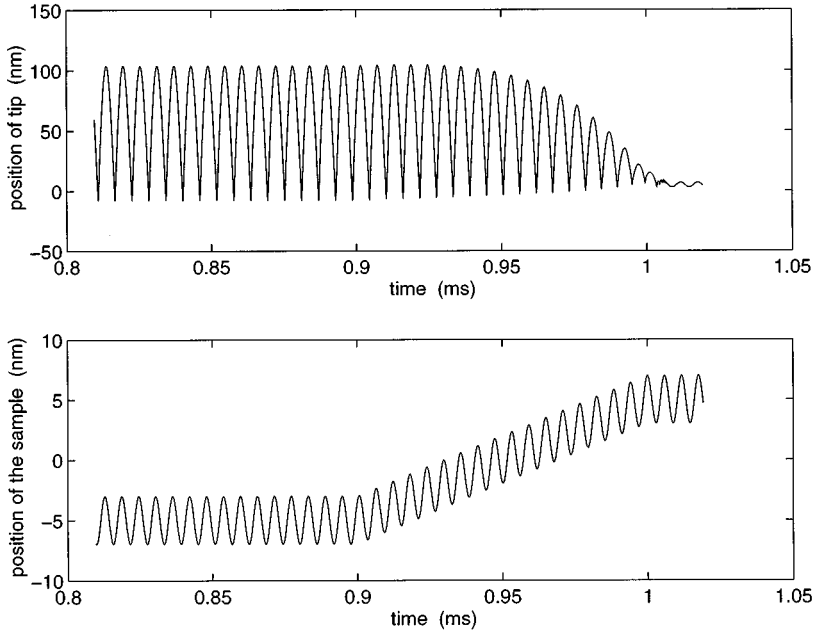

FIG. 10. Gradually increasing σ from -0.5 to 5 nm while driving the sample slightly *below* resonance $\beta=2$ nm, $n=0.97$.

effects in numerical simulations using the full tip-sample interaction. Figures 10 and 11 show the trajectory of the tip subject to a slow change in σ at subresonant and superresonant driving frequencies respectively. In the subresonant case, a decrease of the amplitude of vibration is observed, leading to the tip getting stuck by adhesion, whereas at an excitation frequency above the resonance condition the amplitude increases to a new steady-state amplitude. Although the transition does not proceed strictly adiabatically, resulting in a delay between the change in the tip-cantilever offset and the change in amplitude, the amplitude response behaves as predicted by the single-impact analytical solution of the instantaneous-impact model.

V. CONCLUSION

In this paper we have analyzed intermittent-contact mode AFM from the point of view that the nonlinearity introduced by the drastic increase of stiffness on impact from that of the cantilever to that of the tip-sample contact is crucial to its dynamics. As a result of the disparity between the two stiffnesses the time the tip and sample spend in contact is brief compared to the time between two consecutive impacts and may be brief compared to the driving period. If the latter is the case, the dynamics can be approximately described by an idealized impact law, which instantaneously reverses the relative velocity of the tip and the sample. Hence, it is the energy loss on impact rather than the exact form of the forces producing this rapid acceleration which is crucial for the description of the dynamics resulting from such impacts.

A modification of the coefficient-of-restitution law incorporating adhesion was considered, allowing for two independent forms of energy loss: a loss of energy proportional to the kinetic energy of the tip in the frame where the sample is at rest and an absolute loss of energy per impact, modeling

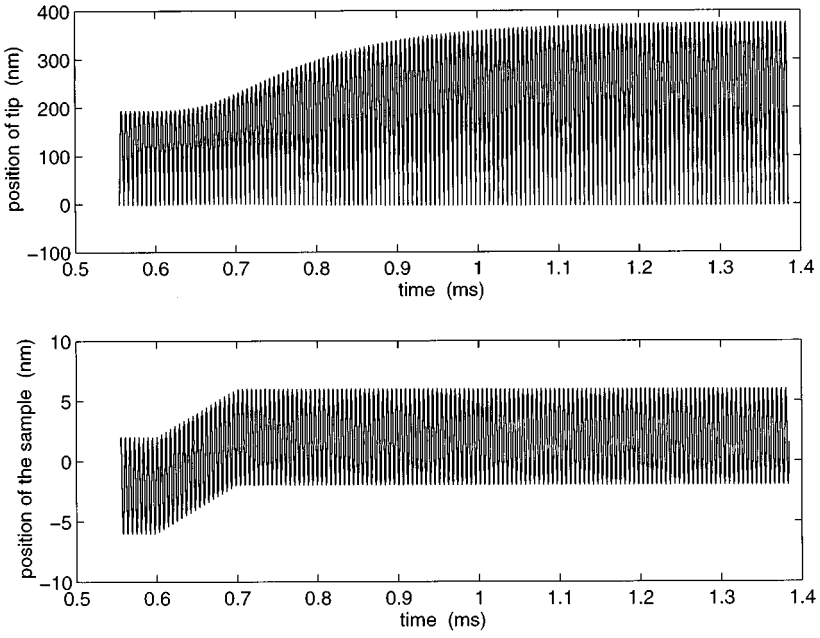

FIG. 11. Gradually increasing σ from -2 to 2 nm while driving the sample slightly *above* resonance $\beta=4$ nm, $n=1.01$.

the effects of adhesion. It was found that the single impact orbits for this impact law are similar to those of the original coefficient-of-restitution law, except at low driving amplitudes and low driving frequencies, where the tip remains ''stuck to the sample'' by adhesion.

A model of the tip-sample interaction based on the JKR model of elastic contact but incorporating the effects of a liquid meniscus between tip and the sample was used to determine the form of the impact law. It was found to follow closely the modified impact law in the presence of adhesion. Furthermore, the assumption that the time of impact is brief compared to the driving period was found to be justified for driving frequencies up to an order of magnitude higher than the free frequency of vibration of the cantilever.

The conclusion that energy dissipation on impact is of prime importance for the dynamics of intermittent-contact mode AFM implies that it may be possible to use such a setup to develop an experimental tool for imaging and characterizing local energy dissipation on impact, since variations in the steady-state amplitude of the cantilever could be used to image the energy loss at the corresponding impact velocities. More importantly, by measuring the amplitudes of vibration of the cantilever and the sample at different subharmonic resonances the impact law can be determined. On resonance the impacts occur when the sample velocity is at a maximum; hence the impact phase is known and from the amplitudes of vibration of the tip and the sample, the driving frequency, and the free frequency of vibration of the cantilever the velocities of the tip before and after impact relative to the platform can be determined. By varying the driving frequency and exciting different subharmonics this relation can be measured over a range of velocities and the impact law be checked experimentally. This information about the local energy dissipation on the sample may also yield new results concerning the dynamic tip-sample interaction.

ACKNOWLEDGMENTS

Many thanks to S. Biswas, O. V. Kolosov, and J. B. Pethica for discussions and criticism. Financial support from the HCM Grant ''Atomic Force Microscopy and Microacoustics'' No. ERBCHRXCT940668 is gratefully acknowledged.

[1] G. Binnig, C. Quate, and C. Gerber, Phys. Rev. Lett. **56**, 930 (1986).
[2] N. Burnham and R. Colton, in *Scanning Tunneling Microscopy and Spectroscopy*, edited by D. Bonnel (VCH, New York, 1993), Chap. 7, pp. 191–249.
[3] R. Wiesendanger, *Scanning Probe Microscopy and Spectroscopy: Methods and Applications* (Cambridge University Press, Cambridge, 1994).
[4] N. Burnham *et al.*, J. Vac. Sci. Technol. B **14**, 1308 (1996).
[5] G. Chen, R. Warmack, A. Huang, and T. Thundat, J. Appl. Phys. **78**, 1465 (1995).
[6] B. Anczykowski, D. Krüger, and H. Fuchs, Phys. Rev. B **53**, 15 485 (1996).
[7] J. Spatz *et al.*, Nanotechnology **6**, 40 (1995).
[8] J. Chen, R. Workman, D. Sarid, and R. Höper, Nanotechnology **5**, 199 (1994).
[9] D. Sarid, J. Chen, and R. Workman, Comput. Mater. Sci. **3**, 475 (1995).
[10] C. Putman *et al.*, Appl. Phys. Lett. **64**, 2454 (1994).
[11] N. Burnham *et al.*, Nanotechnology **8**, 67 (1997).
[12] N. Burnham, A. Kulik, G. Gremaud, and G.A.D. Briggs, Phys. Rev. Lett. **74**, 5092 (1995).
[13] S. Shaw, J. Appl. Mech. **85**, 453 (1985).
[14] S. Shaw, J. Appl. Mech. **85**, 459 (1985).
[15] S. Shaw and P. Holmes, J. Sound Vib. **90**, 122 (1983).
[16] S. Hogan, Proc. R. Soc. London, Sec. A **425**, 441 (1989).
[17] J. Thompson, Proc. R. Soc. London, Sec. A **387**, 407 (1983).
[18] J. Thompson, A. Bokaian, and R. Ghaffari, Trans. ASME, J. Energy Resour. Technol. **106**, 191 (1984).
[19] Philos. Trans. R. Soc. London, Ser. A **347** (1994).
[20] G. Whiston, J. Sound Vib. **118**, 395 (1987).
[21] J. Guckenheimer and P. Holmes, *Non-Linear Oscillations, Dynamical Systems and Bifurcations of Vector Fields, 2nd ed.*, Vol. 42 of *Applied Mathematical Sciences* (Springer-Verlag, Heidelberg, 1986).
[22] J. Israelachvili, *Intermolecular and Surface Forces* (Academic, London, 1991).
[23] K. Johnson, *Contact Mechanics* (Cambridge University Press, Cambridge, 1985).
[24] K. Johnson, K. Kendall, and A. Roberts, Proc. R. Soc. London, Ser. A **324**, 301 (1971).
[25] M. Adams and B. Edmundson, in *Tribology in Particulate Environments*, edited by B. Briscoe and M. Adams (Adam Hilger, Bristol, 1987), Chap. 2.4, pp. 154–172.
[26] A. Adamson, *Physical Chemistry of Surfaces* (Wiley, New York, 1976).
[27] H. Brenner, Chem. Eng. Sci. **16**, 242 (1961).
[28] S. O'Shea, M. Welland, and J. Pethica, Chem. Phys. Lett. **223**, 336 (1994).
[29] J.B. Pethica and S. Biswas (unpublished).
[30] D. Maugis, J. Colloid Interface Sci. **150**, 243 (1992).
[31] O. Kolosov and K. Yamanaka, Jpn. J. Appl. Phys. **32**, 1095 (1993).
[32] A. Kapoor (private communication).
[33] K. Yamanaka (private communication).
[34] For large n impact velocities will in general be correspondingly larger.
[35] N. Burnham (private communication).
[36] Negative values of σ correspond to a tensile offset.